Portland State University

PDXScholar

TREC Final Reports

Transportation Research and Education Center (TREC)

9-2013

Modeling of DC Link Capacitor Current Ripple for Electric Vehicle Traction Converter

Lei Jin
Oregon State University

Julia Zhang
Oregon State University

Follow this and additional works at: https://pdxscholar.library.pdx.edu/trec_reports

Part of the Transportation Commons, Urban Studies Commons, and the Urban Studies and Planning Commons

Let us know how access to this document benefits you.

Recommended Citation

Julia Zhang and Lei Jin. Modeling of DC link Capacitor Current Ripple for Electric Vehicle Traction Converter. OTREC-SS-634. Portland, OR: Transportation Research and Education Center (TREC), 2010. https://doi.org/10.15760/trec.40

This Report is brought to you for free and open access. It has been accepted for inclusion in TREC Final Reports by an authorized administrator of PDXScholar. Please contact us if we can make this document more accessible: pdxscholar@pdx.edu.

OREGON
TRANSPORTATION
RESEARCH AND
EDUCATION CONSORTIUM

OTREC

FINAL REPORT

Modeling of DC Link Capacitor Current Ripple For Electric Vehicle Traction Converter

OTREC-SS-634
September 2013

A National University Transportation Center sponsored by the U.S. Department of Transportation's Research and Innovative Technology Administration

MODELING OF DC LINK CAPACITOR CURRENT RIPPLE FOR ELECTRIC VEHICLE TRACTION CONVERTER

Draft Report

OTREC-SS-634

by

Lei Jin
Advisor: Julia Zhang
Oregon State University

for

Oregon Transportation Research
and Education Consortium (OTREC)
P.O. Box 751
Portland, OR 97207

September 2013

Technical Report Documentation Page

1. Report No. OTREC-SS-634	2. Government Accession No.	3. Recipient's Catalog No.
4. Title and Subtitle Wider dissemination of household travel survey data using geographical perturbation methods		5. Report Date September, 2013 6. Performing Organization Code
7. Author(s) Lei Jin, Julia Zhang		8. Performing Organization Report No.
9. Performing Organization Name and Address Oregon State University		10. Work Unit No. (TRAIS) 11. Contract or Grant No.
12. Sponsoring Agency Name and Address Oregon Transportation Research and Education Consortium (OTREC) P.O. Box 751 Portland, Oregon 97207		13. Type of Report and Period Covered 14. Sponsoring Agency Code
15. Supplementary Notes		
16. Abstract		
17. Key Words	18. Distribution Statement No restrictions. Copies available from OTREC: www.otrec.us	

19. Security Classification (of this report) Unclassified	20. Security Classification (of this page) Unclassified	21. No. of Pages 13	22. Price

Modeling of DC Link Capacitor Current Ripple for Electric Vehicle Traction Converter

Lei Jin
Advisor: Julia Zhang
School of Electrical Engineering and Computer Science
Oregon State University

09/28/2013

Table of Contents

1. Introduction

Contemporary Full Hybrid Electric Vehicle/Plug-in Hybrid Electric Vehicle/Battery Electric Vehicle (FHEV/PHEV/BEV) products use one or more DC/AC power converters, also known as traction inverters, to convert the DC voltage/current provided by the traction battery to the AC voltage/current to drive the traction motor(s). Large and bulky DC link capacitors are used at the input of the traction inverter to provide a smooth DC input voltage. Those DC link capacitors, occupying almost 50% of the space in the whole package, can contribute to more than 20% of the total cost of the traction inverter. They are generally over-designed to assure a large safety margin during the fast transient operation of the electric machine(s). However, it is not well understood how the capacitor size reduction affects the electric machine drive system performance and operation stability. This work presents the numerical method of calculating the DC link capacitor current ripple of the traction converter for electric vehicle applications. The effect of internal resistance of the input voltage source is taken into account for the math modeling. This provides guidance to the minimum boundary of the DC link capacitor size of traction power inverters for the application of battery electric vehicles.

Figure 1 shows a typical topology of the electric machine drive system for an FHEV/PHEV. The DC/DC converter, boosting the traction battery voltage to a higher DC voltage, may not exist for a BEV. The two traction inverters convert the DC voltage to AC voltage to drive electric machines. A BEV may only have one traction inverter and one electric machine.

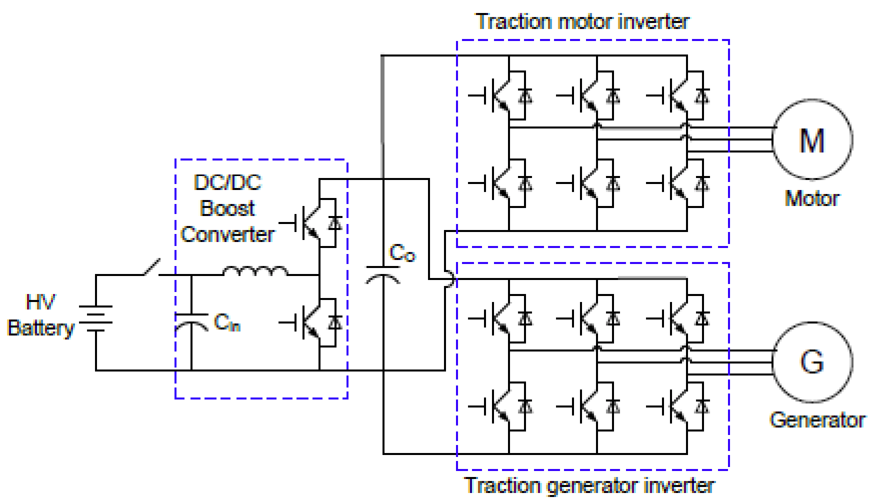

Figure 1 Electric machine drive topology on FHEV/PHEV/BEV

2. Space Vector PWM Fundamentals

We introduce the space vector pulse width modulation (SVPWM) fundamentals first. Secondly, we discuss the numerical method of calculating the root mean square (RMS) value of the capacitor current ripple. Figure 2 shows a three-phase voltage source inverter (VSI). The load of the inverter is a back electromotive force (EMF) source in series with an inductor to represent a three-phase electric machine. For each of the three phases, Status “1” means that the top switch turns on and vice versa. In Status “0” the bottom switch turns on. Figure 3 shows all eight voltage vectors that a three-phase VSI may have. They are (100), (110), (010), (011), (001), (101), (111) and (000). Among the eight voltage vectors, six are the active voltage vectors and two are the zero-voltage vectors (000, 111).

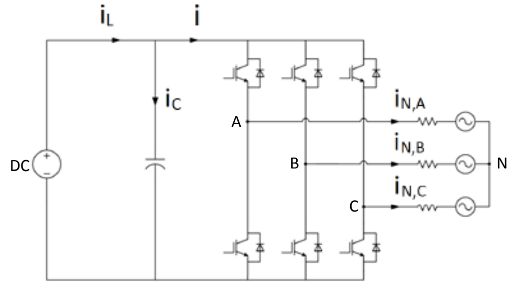

Figure 2 Three-phase voltage source inverter

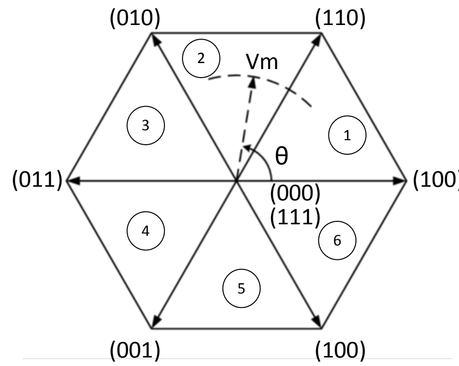

Figure 3 Six active voltage vectors and two zero-voltage vectors

A rotating voltage vector command may be expressed as:

$$\overrightarrow{V_m} = V_m exp(j\theta) \quad (1)$$

$$\theta = \omega t \quad (2)$$

where V_m is the magnitude of the command voltage vector, θ the angle of the voltage vector, and ω the electrical angular velocity of the voltage vector. Various definitions exist for the modulation index. In our study, we define the modulation index as:

$$M = \frac{V_m}{0.5V_{dc}} \quad (3)$$

where V_{dc} is the DC bus voltage. For this definition, the maximum value of the modulation index is $2/\sqrt{3}$ when the six-step control is applied to the load.

In Figure 3, the rotating command voltage vector lies in the second sector. In this case, this command voltage vector will be generated by the four voltage vectors in the second sector: 110, 010, 000 and 111. For the SVPWM algorithm, the duty cycle of each voltage vector may be written as:

$$D_{(010)} = \frac{t_{(010)}}{T_s} = \frac{\sqrt{3}M}{2}\sin(\theta - \frac{\pi}{3}) \quad (4)$$

$$D_{(110)} = \frac{t_{(110)}}{T_s} = \frac{\sqrt{3}M}{2}\sin(\theta + \frac{\pi}{3}) \quad (5)$$

$$D_{(000)} = D_{(111)} = 0.5(1 - D_{(010)} - D_{(110)}) \quad (6)$$

where T_s is one switching cycle, $t_{(010)}$ and $t_{(110)}$ are the time durations when vectors 010 and 110 are applied, respectively.

3. Average Value of Inverter Input Current

For the "Y" connection load shown in Figure 1, the sum of the three phase currents is zero:

$$i_{N,A} + i_{N,B} + i_{N,C} \equiv 0 \quad (7)$$

In the time domain, the three phase currents can be expressed as:

$$\mathrm{i}_{\mathrm{N,A}} = I_m \cos(\theta - \varphi) \quad (8)$$

$$i_{N,B} = I_m \cos(\theta - \frac{2\pi}{3} - \varphi) \quad (9)$$

$$i_{N,C} = I_m \cos(\theta + \frac{2\pi}{3} - \varphi) \tag{10}$$

where I_m is the magnitude of phase current, ϕ denotes the angle that the current is lagging the voltage. The space vector form of the three-phase current is written as:

$$\overrightarrow{I_m} = I_m exp\{j(\theta - \varphi)\} \tag{11}$$

Figure 4 shows the inverter input current and the three-phase switching signals in two switching cycles.

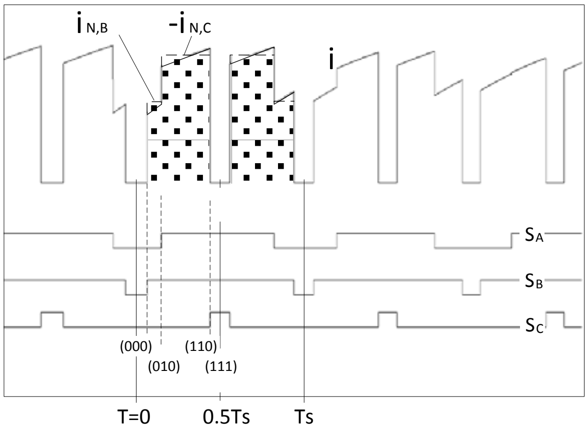

Figure 4. Inverter input current and three-phase switching signals

Assuming that the instantaneous value of the inverter input current is *i*, the average value of the inverter input current in one switching cycle, i_{avg}, can be expressed as:

$$i_{avg} = \frac{2}{T_s}\int_0^{\frac{1}{2}T_s} i(t)dt \tag{12}$$

$$i_{avg} = D_{(010)}i_{N,B} - D_{(110)}i_{N,C} \tag{13}$$

Substituting Eqs. (3) to (6) and Eqs. (8) to (10) into Eq. (13), the average inverter input current may be rewritten as:

$$i_{avg} = \frac{\sqrt{3}M}{2}\sin(\theta - \frac{\pi}{3}) \cdot I_m \cos\left(\theta - \frac{2\pi}{3} - \varphi\right) - \frac{\sqrt{3}M}{2}\sin(\theta + \frac{\pi}{3}) \cdot I_m \cos\left(\theta + \frac{2\pi}{3} - \varphi\right) \tag{14}$$

The above equation may be further simplified as:

$$i_{avg} = I_{avg} = \frac{3}{4} I_m M\cos\varphi \tag{15}$$

It can be seen that the average value of the inverter input current is a function of the phase current magnitude, modulation index and the angle between the current and voltage vectors - in other words, the power factor.

4. RMS Value of Inverter Input Current

The RMS value of the inverter input current in one switching cycle T_s can be expressed as:

$$i_{rms}^2 = \frac{2}{T_s}\int_0^{\frac{1}{2}T_s} i^2 dt \tag{16}$$

Substituting Eqs. (3) to (6) and Eqs. (8) to (10) into Eq. (16), the RMS inverter input current may be rewritten as,

$$i_{rms}^2 = D_{(010)} i_{N,B}^2 + D_{(110)} i_{N,C}^2 \tag{17}$$

The lowest harmonic in the inverter input current is six times the fundamental frequency of the phase current, as shown in Figure 5.

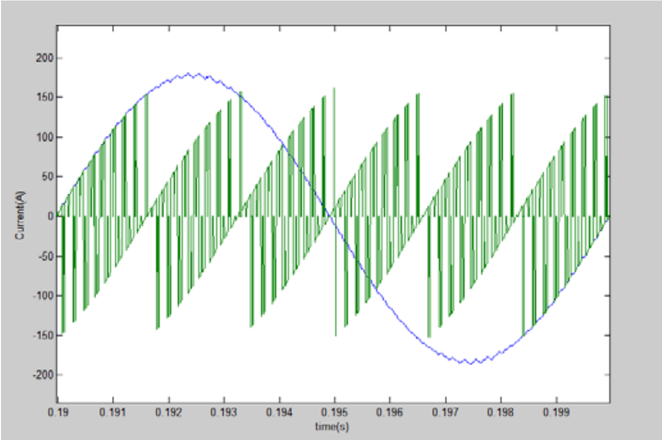

Figure 5. Inverter input current for pure resistive load

The RMS value of the inverter input current can be written as:

$$I_{rms}^2 = \frac{3}{\pi}\int_{\frac{\pi}{3}}^{\frac{2\pi}{3}} i_{rms}^2 \, d\theta \tag{18}$$

Substituting Eqs. (3) to (6) and Eqs. (8) to (10) into Eq. (18), the RMS value of the inverter input current I_{rms} can be written as:

$$I_{rms}^2 = \frac{3}{\pi}\int_{\frac{\pi}{3}}^{\frac{2\pi}{3}} (D_{(010)} i_{N,B}^2 + D_{(110)} i_{N,C}^2) d\theta \tag{19}$$

$$I_{rms}^2 = \frac{3}{\pi}\int_{\frac{\pi}{3}}^{\frac{2\pi}{3}} \left\{\frac{\sqrt{3}M}{2} sin(\theta - \frac{\pi}{3}) \left[I_m \, cos(\theta - \frac{2\pi}{3} - \varphi)\right]^2 + \frac{\sqrt{3}M}{2} sin(\theta + \frac{\pi}{3}) \left[I_m \, cos(\theta + \frac{2\pi}{3} - \varphi)\right]^2\right\} d\theta \tag{20}$$

$$I_{rms} = \frac{I_m}{\sqrt{2}}\sqrt{\frac{2\sqrt{3}}{\pi} M \left(\frac{1}{4} + \cos^2\varphi\right)} \tag{21}$$

where I_m is the peak value of the phase current, *M* the modulation index, *φ* the angle between the current vector and the voltage vector.

5. RMS Value of DC Link Capacitor Current Ripple

The input inverter current, i, is composed of the AC and DC component:

$$i = i_{ac} + i_{dc} = i_{ac} + i_{avg} \tag{20}$$

The DC component is equal to the average value obtained in Eq. (15). The RMS value of the inverter input current can be expressed as:

$$I_{rms}^2 = I_{ac,rms}^2 + I_{dc}^2 = I_{ac,rms}^2 + I_{avg}^2 \tag{21}$$

Let us assume the AC component is absorbed by the DC link capacitor completely.

$$I_{ac,rms}^2 = I_{C,rms}^2 \tag{22}$$

The RMS value of the capacitor current may be written as:

$$I_{C,rms}^2 = I_{rms}^2 - I_{avg}^2 \tag{23}$$

Substituting Eqs. (15) and (21) into Eq. (23), the RMS value of capacitor current ripple can be written as:

$$I_{C,rms} = \sqrt{I_{N,rms}^2 \frac{2\sqrt{3}}{\pi} M \left(\frac{1}{4} + cos^2\,\varphi\right) - \left(\frac{3}{4} I_m\, M cos\,\varphi\right)^2} \tag{24}$$

$$I_{C,rms} = I_{N,rms} \sqrt{2M\left[\frac{\sqrt{3}}{4\pi} + \cos^2\varphi\left(\frac{\sqrt{3}}{\pi} - \frac{9}{16}M\right)\right]} \tag{25}$$

Figure 6 shows the capacitor current ripple constant versus various power factor and modulation index. It can be seen that the maximum modulation index does not necessarily yield the highest capacitor current ripple.

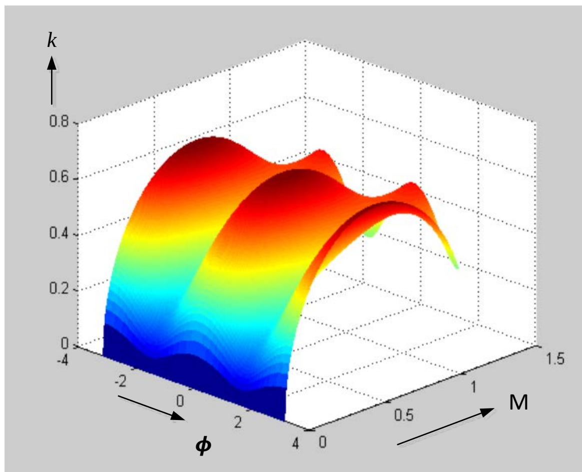

Figure 6. Capacitor current ripple constant vs. power factor and modulation index

6. Numerical Method of Calculating Instantaneous Capacitor Current Ripple

First, we calculate the instantaneous three-phase current using a pure inductance load. Figure 7 shows six switching patterns. The "green" power switches are the switches which are conducting current.

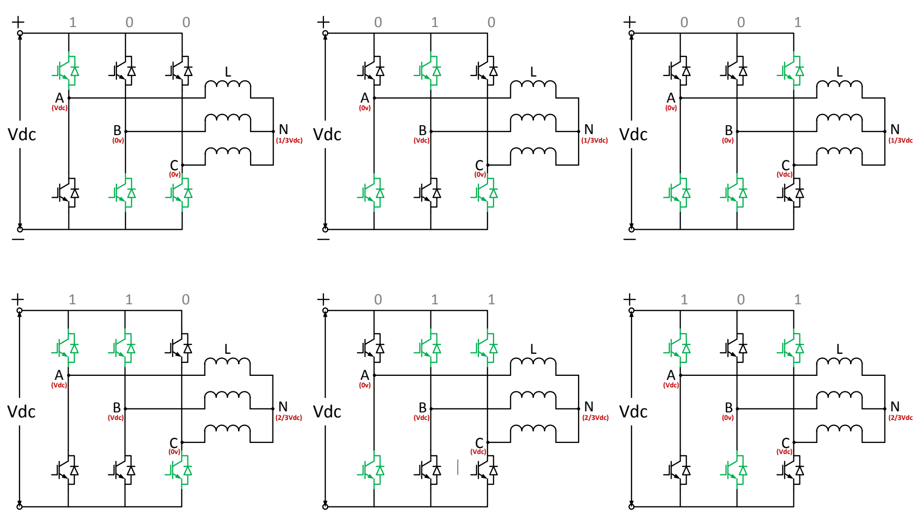

Figure 7. Six switching patterns (L load)

The current change in one switching cycle is given by Eqs. (26) to (31) to the above six switching patterns. When either one of the two zero-voltage vectors (000 and 111) is applied, the three-phase current maintains unchanged in one switching cycle.

$\begin{cases} \Delta i_A = \frac{2V_{dc}}{3L}\Delta t \\ \Delta i_B = -\frac{V_{dc}}{3L}\Delta t \\ \Delta i_C = -\frac{V_{dc}}{3L}\Delta t \end{cases}$	(26)	$\begin{cases} \Delta i_A = -\frac{V_{dc}}{3L}\Delta t \\ \Delta i_B = \frac{2V_{dc}}{3L}\Delta t \\ \Delta i_C = -\frac{V_{dc}}{3L}\Delta t \end{cases}$	(27)	$\begin{cases} \Delta i_A = -\frac{V_{dc}}{3L}\Delta t \\ \Delta i_B = -\frac{V_{dc}}{3L}\Delta t \\ \Delta i_C = \frac{2V_{dc}}{3L}\Delta t \end{cases}$	(28)
$\begin{cases} \Delta i_A = \frac{V_{dc}}{3L}\Delta t \\ \Delta i_B = \frac{V_{dc}}{3L}\Delta t \\ \Delta i_C = -\frac{2V_{dc}}{3L}\Delta t \end{cases}$	(29)	$\begin{cases} \Delta i_A = -\frac{2V_{dc}}{3L}\Delta t \\ \Delta i_B = \frac{V_{dc}}{3L}\Delta t \\ \Delta i_C = \frac{V_{dc}}{3L}\Delta t \end{cases}$	(30)	$\begin{cases} \Delta i_A = \frac{V_{dc}}{3L}\Delta t \\ \Delta i_B = -\frac{2V_{dc}}{3L}\Delta t \\ \Delta i_C = \frac{V_{dc}}{3L}\Delta t \end{cases}$	(31)

where L is the inductance of the load.

Figure 8 shows six switching patterns with an electric machine load. The electric machine load is represented by an RL load in series with a back EMF voltage source. The current change in one switching cycle is given by Eqs. (32) to (37).

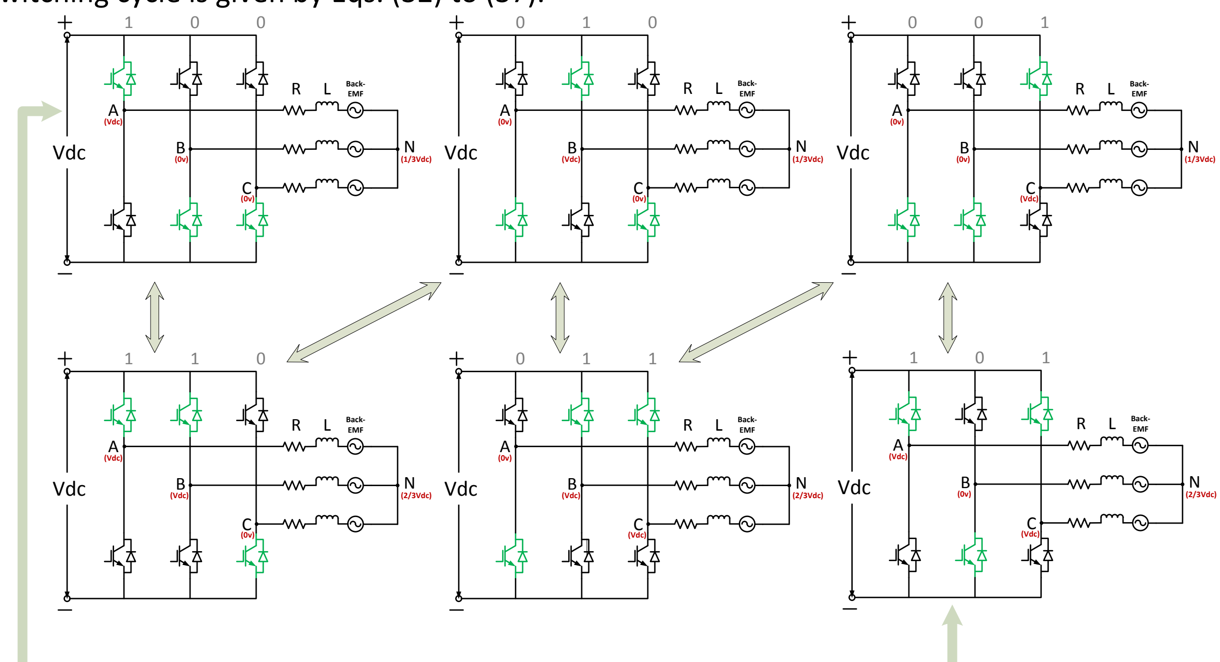

Figure 8. Six switching patterns (electric machine load)

100	$\begin{cases} \Delta i_A = \dfrac{2V_{dc} - 3E_m\cos(\omega t_0 + \varphi) - 3Ri_{A0}}{3L}\Delta t \\ \Delta i_B = \dfrac{-V_{dc} - 3E_m\cos(\omega t_0 + \varphi - 2\pi/3) - 3Ri_{B0}}{3L}\Delta t \\ \Delta i_C = \dfrac{-V_{dc} - 3E_m\cos(\omega t_0 + \varphi + 2\pi/3) - 3Ri_{C0}}{3L}\Delta t \end{cases}$	(32)
110	$\begin{cases} \Delta i_A = \dfrac{V_{dc} - 3E_m\cos(\omega t_0 + \varphi) - 3Ri_{A0}}{3L}\Delta t \\ \Delta i_B = \dfrac{V_{dc} - 3E_m\cos(\omega t_0 + \varphi - 2\pi/3) - 3Ri_{B0}}{3L}\Delta t \\ \Delta i_C = \dfrac{-2V_{dc} - 3E_m\cos(\omega t_0 + \varphi + 2\pi/3) - 3Ri_{C0}}{3L}\Delta t \end{cases}$	(33)
010	$\begin{cases} \Delta i_A = \dfrac{-V_{dc} - 3E_m\cos(\omega t_0 + \varphi) - 3Ri_{A0}}{3L}\Delta t \\ \Delta i_B = \dfrac{2V_{dc} - 3E_m\cos(\omega t_0 + \varphi - 2\pi/3) - 3Ri_{B0}}{3L}\Delta t \\ \Delta i_C = \dfrac{-V_{dc} - 3E_m\cos(\omega t_0 + \varphi + 2\pi/3) - 3Ri_{C0}}{3L}\Delta t \end{cases}$	(34)
011	$\begin{cases} \Delta i_A = \dfrac{-2V_{dc} - 3E_m\cos(\omega t_0 + \varphi) - 3Ri_{A0}}{3L}\Delta t \\ \Delta i_B = \dfrac{V_{dc} - 3E_m\cos(\omega t_0 + \varphi - 2\pi/3) - 3Ri_{B0}}{3L}\Delta t \\ \Delta i_C = \dfrac{V_{dc} - 3E_m\cos(\omega t_0 + \varphi + 2\pi/3) - 3Ri_{C0}}{3L}\Delta t \end{cases}$	(35)
001	$\begin{cases} \Delta i_A = \dfrac{-V_{dc} - 3E_m\cos(\omega t_0 + \varphi) - 3Ri_{A0}}{3L}\Delta t \\ \Delta i_B = \dfrac{-V_{dc} - 3E_m\cos(\omega t_0 + \varphi - 2\pi/3) - 3Ri_{B0}}{3L}\Delta t \\ \Delta i_C = \dfrac{2V_{dc} - 3E_m\cos(\omega t_0 + \varphi + 2\pi/3) - 3Ri_{C0}}{3L}\Delta t \end{cases}$	(36)
101	$\begin{cases} \Delta i_A = \dfrac{V_{dc} - 3E_m\cos(\omega t_0 + \varphi) - 3Ri_{A0}}{3L}\Delta t \\ \Delta i_B = \dfrac{-2V_{dc} - 3E_m\cos(\omega t_0 + \varphi - 2\pi/3) - 3Ri_{B0}}{3L}\Delta t \\ \Delta i_C = \dfrac{V_{dc} - 3E_m\cos(\omega t_0 + \varphi + 2\pi/3) - 3Ri_{C0}}{3L}\Delta t \end{cases}$	(37)

where R is the electric machine winding resistance, L the inductance, E_{m} the back EMF, i_{A0}, i_{B0} and i_{C0} are the initial value of the three-phase current at the beginning of one switching cycle.

Figure 9 shows the flow chart of the numerical method of calculating the instantaneous three-phase current, inverter input current and capacitor current. Figures 10-12 show the three-phase current, inverter input current and capacitor voltage ripple for three different types of load using the numerical method.

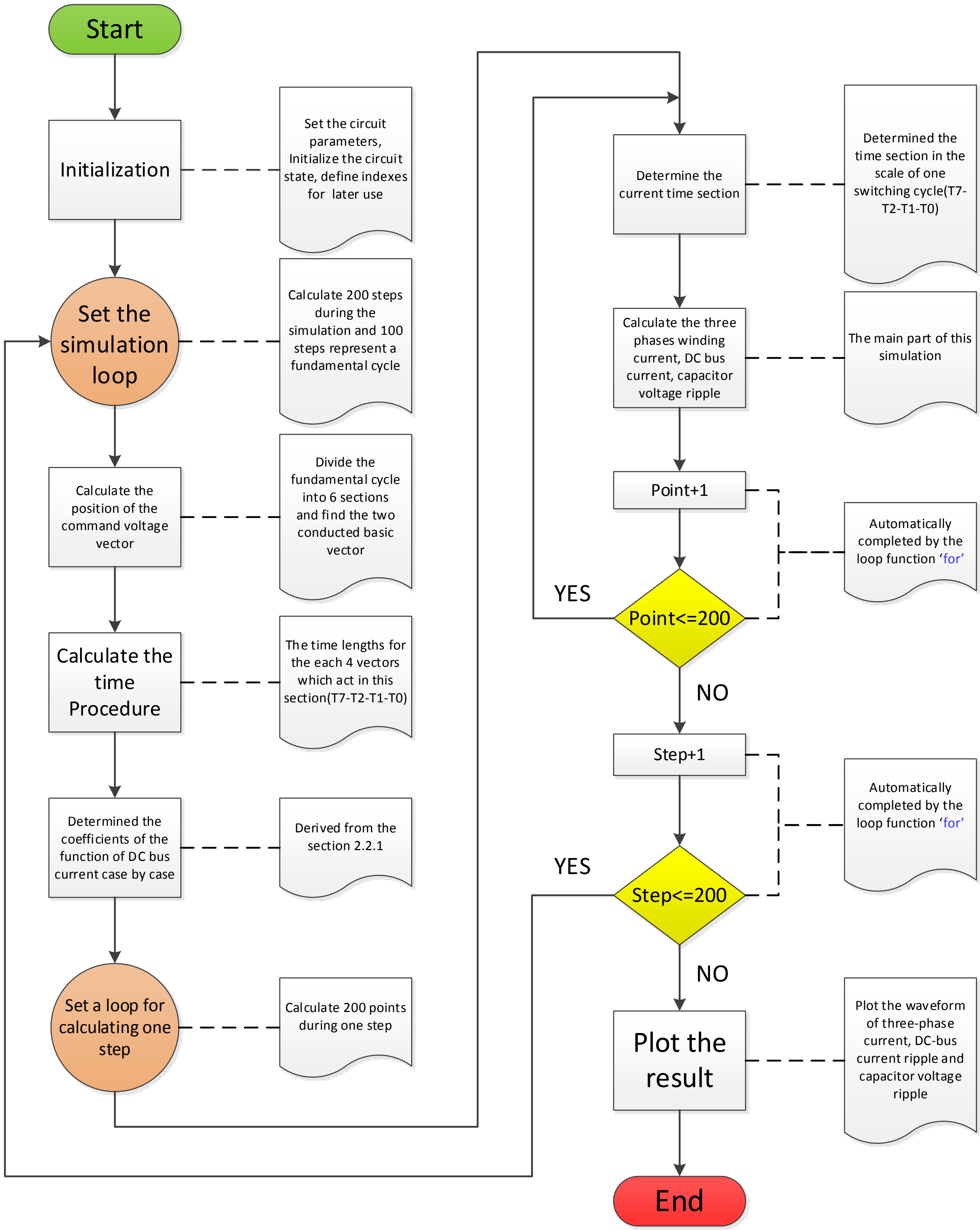

Figure 9. Numerical method of reconstructing instantaneous three-phase current

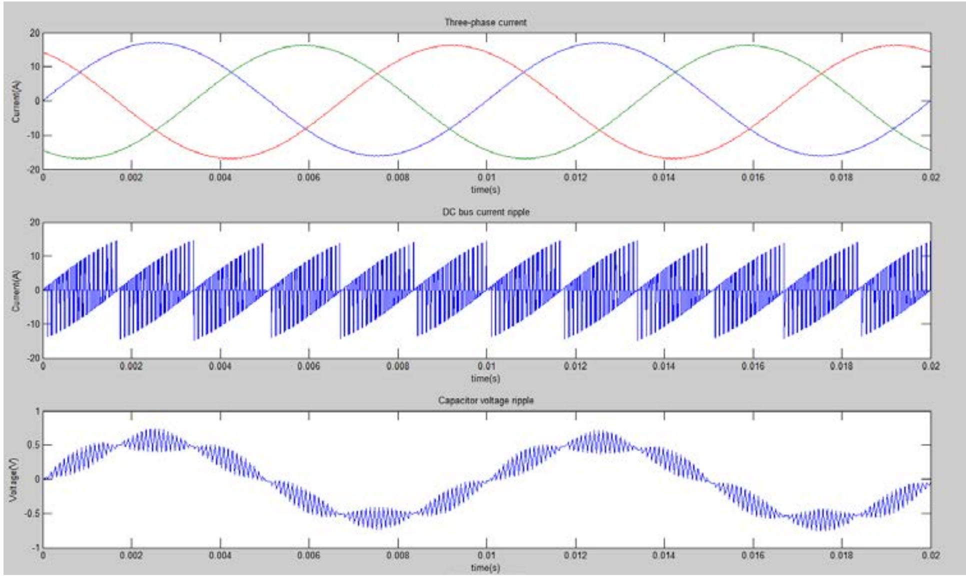

Figure 10. Instantaneous waveforms with L load

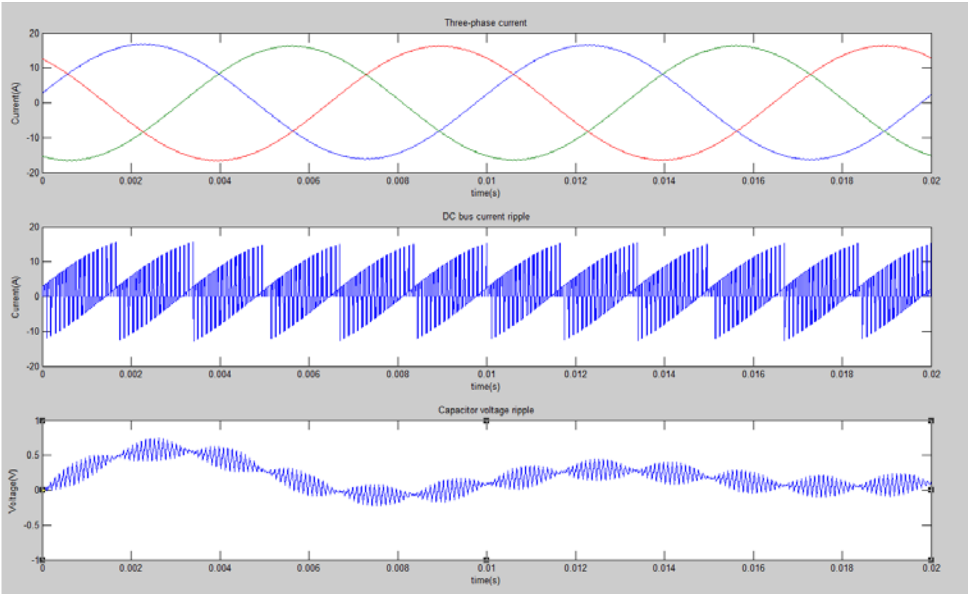

Figure 11. Instantaneous waveforms with RL load

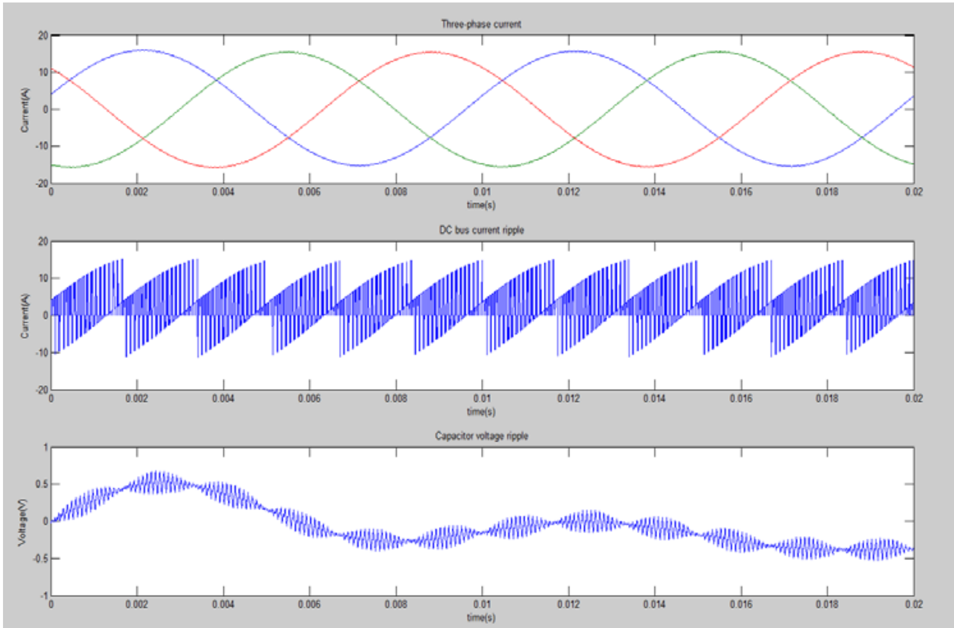

Figure 12. Instantaneous waveforms with electric machine model

7. Analysis for Non-ideal Voltage Source

In the previous analysis, we have assumed that the input voltage source is an ideal source without any internal resistance. In the real-world application, the input voltage source always has a small internal resistance. That is also why a large DC link capacitor is needed to provide smooth input voltage to the three-phase inverter. For the following analysis, we will take into account the effect of the voltage source internal resistance. In Figure 13, the input voltage source is represented by an ideal voltage source in series with an internal resistance.

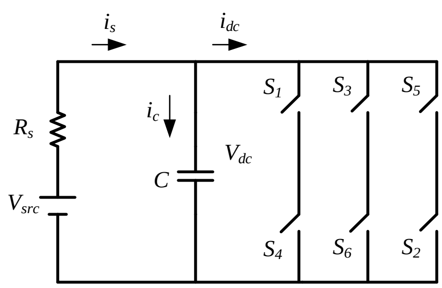

Figure 13. Model of non-ideal input voltage source

For the system shown in Figure 12, Eq. (38) exists:

$$\begin{cases} i_{dc} = i_s - i_c \\ i_c = C\dfrac{dV_{dc}}{dt} \\ V_{dc} = V_{src} - R_s i_s \end{cases} \tag{38}$$

where C is the capacitance of the DC link capacitor, R_s is the internal resistance of the input voltage source. In Eq. (25), we assume the input voltage V_{src}, its internal resistance R_s and the capacitance C are known. In addition, the inverter input current i_{dc} can be calculated by Eq. (39), regarded as a known variable.

$$i_{dc} = i_A S_A + i_B S_B + i_C S_C \tag{38}$$

where i_A, i_B and i_C are the three-phase current, S_A, S_B and S_C are the three-phase switching function. The three-phase current may be obtained using the numerical method presented in the previous part. Therefore, the capacitor current and the voltage source current may be written as:

$$\frac{di_c}{dt} + \frac{i_c}{R_s C} + \frac{di_{dc}}{dt} = 0 \tag{39}$$

$$i_s = i_C + i_{dc} \tag{40}$$

Eqs. (39) and (40) are later used to calculate the instantaneous capacitor current and the source current in Matlab. Figure 14 shows the results of the voltage source current, capacitor voltage and current using the numerical method. Figure 15 shows the flow chart of the Matlab script.

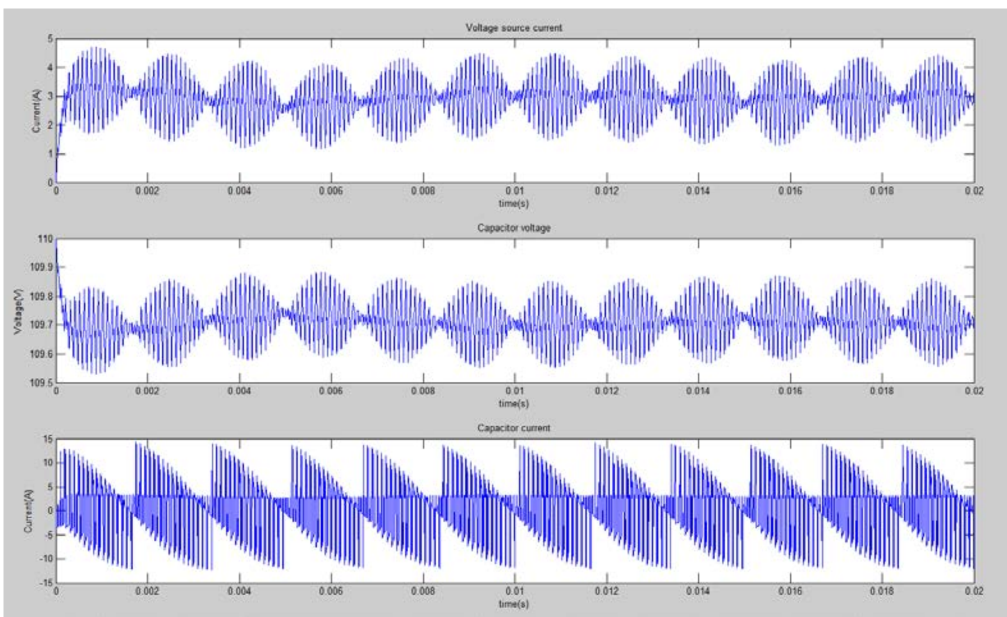

Figure 14. Voltage source ripple and capacitor current ripple using numerical method

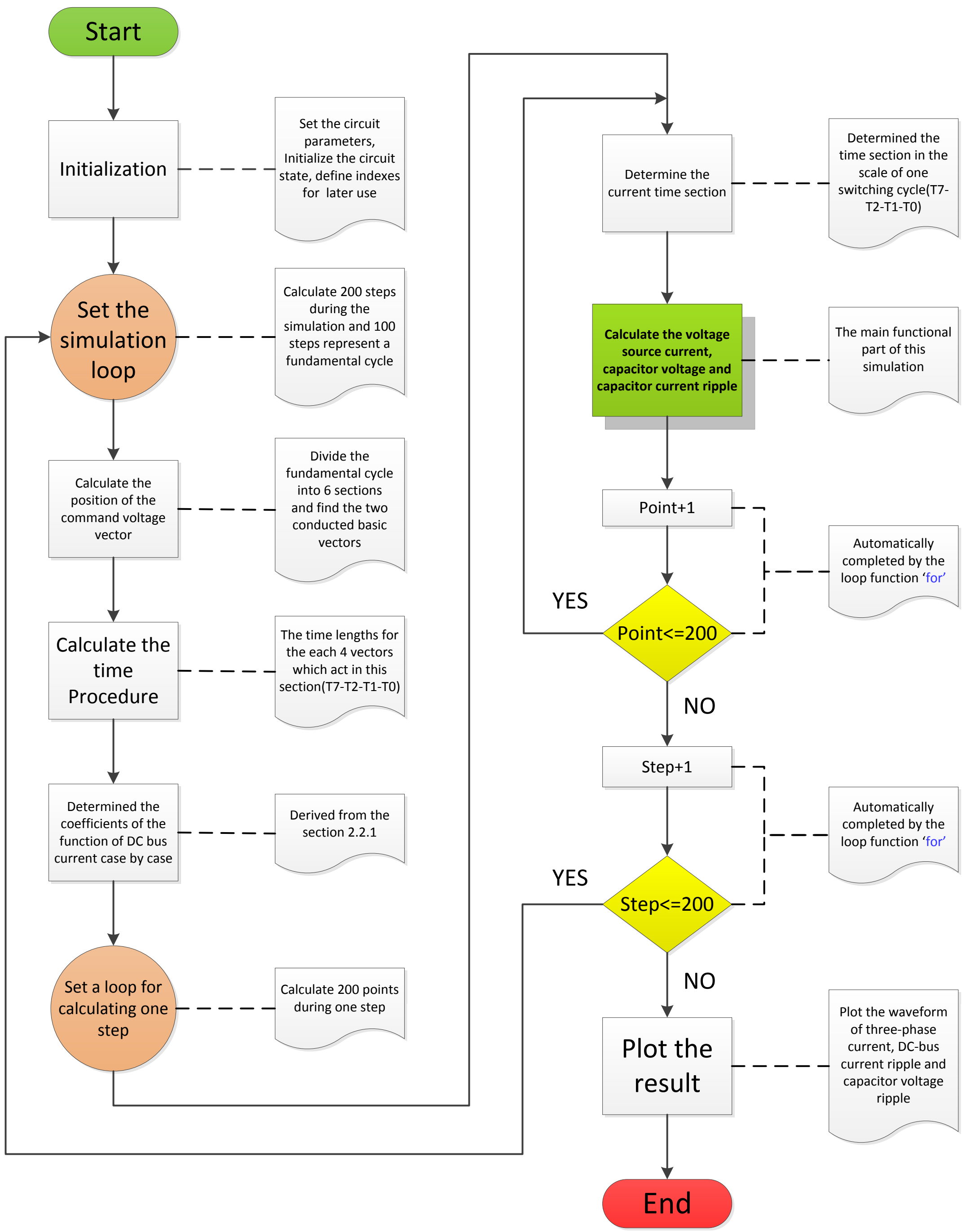

Figure 15. Flow chart of calculating capacitor current and voltage source current for non-ideal voltage source

8. Summary

This report first reviews the challenges that the bulky DC link capacitor of the electric vehicle traction inverter presents to further power density increase and cost reduction. Then this work presents the numerical method of calculating the DC link capacitor current ripple of the traction converter for electric vehicle applications. The effect of internal resistance of the input voltage source is taken into account for the math modeling.

9. References

[1] J. Kolar and S. Round, "Analytical calculation of the RMS current stress on the DC-link capacitor of voltage-PWM converter systems," IEE Proceedings of Electric Power Applications, Vol. 153, No. 4, July 2006.

[2] F. Kieferndorf, M. Förster and T. Lipo, "Reduction of DC-Bus Capacitor Ripple Current with PAM/PWM Converter," IEEE Transactions on Industry Applications, Vol. 40, No. 2, March/April 2004.

[3] J. Zhu and A. Pratt, "Capacitor Ripple Current in an Interleaved PFC Converter," IEEE Transaction on Power Electronics, Vol. 24, No. 6, June 2009.

[4] T.-P Chen, "Common-Mode Ripple Current Estimator for Parallel Three-Phase Inverters," IEEE Transaction on Power Electronics, Vol. 24, No. 5, May 2009.

[5] K. Ramachandrasekhar and S. Srinivas, "Discontinuous Decoupled PWMs for Reduced Current Ripple in a Dual Two-Level Inverter Fed Open-End Winding Induction Motor Drive," IEEE Transaction on Power Electronics, Vol. 28, No. 5, May 2013.

[6] H. van der Broeck, H. C. Skudelny and G. Stanke, "Analysis and Realization of a Pulsewidth Modulator Based on Voltage Space Vectors," IEEE Transactions on Industry Applications, Vol. 24, No. 1, January/February 1988.

[7] J. Kolar, H. Ertl and F. Zach, "Calculation of the Passive and Active Component Stress Of Three Phase PWM Converter Systems with High Pulse Rate," 3rd European Conference on Power Electronics and Applications, pp. 1303-1311, October 1989.

[8] G. Su and L. Tang, "A segmented traction drive system with a small dc bus capacitor," Energy Conversion Congress and Exposition, pp. 2847-2853, September 2012

[9] A. Hava, R. Kerkman and T. Lipo, "Simple Analytical and Graphical Methods for Carrier-Based PWM-VSI Drives," IEEE Transaction on Power Electronics, Vol. 14, No. 1, January 1999

[10] S. Kim, Y. Yoon and S. Sul, "Pulsewidth Modulation Method of Matrix Converter for Reducing Output Current Ripple," IEEE Transaction on Power Electronics, Vol. 25, No. 10, October 2010

[11] B. Vafakhah, J. Salmon and A. Knight, "A New Space-Vector PWM With Optimal Switching Selection for Multilevel Coupled Inductor Inverters," IEEE Transaction on Industrial Electronics, Vol. 57, No. 7, July 2010

[12] M. Gasperi, "Life Prediction Modeling of Bus Capacitors in AC Variable-Frequency Drives," IEEE Transactions on Industry Applications, Vol. 41, No. 6, November/December 2005.

OREGON TRANSPORTATION RESEARCH AND EDUCATION CONSORTIUM

P.O. Box 751
Portland, OR 97207

OTREC is dedicated to stimulating and conducting collaborative multi-disciplinary research on multi-modal surface transportation issues, educating a diverse array of current practitioners and future leaders in the transportation field, and encouraging implementation of relevant research results.